analytical chemistry

ARTICLE

pubs.acs.org/ac

Lateral Flow Immunochromatographic Assay for Sensitive Pesticide Detection by Using Fe_3O_4 Nanoparticle Aggregates as Color Reagents

Chunyan Liu,[†] Qiaojuan Jia,[†] Chunhui Yang,[†] Ruirui Qiao,[†] Lihong Jing,[†] Libing Wang,[*,‡] Chuanlai Xu,[‡] and Mingyuan Gao[*,†]

[†]Institute of Chemistry, Chinese Academy of Sciences, Bei Yi Jie 2, Zhong Guan Cun, Beijing 100190, China

[‡]School of Food Science and Technology, Jiangnan University, Lihu Road 1800, Wuxi, Jiangsu Province, 214122, China

Supporting Information

ABSTRACT: Magnetic Fe_3O_4 particle aggregates were prepared by cross-linking Fe_3O_4 nanoparticles bearing surface carbonyl groups with poly-L-lysine. Upon further coupling with antiparaoxon methyl polyclonal antibody, the resultant particle aggregate-based probes were used in a lateral flow immunochromatographic assay (LFIA) of pesticide residue of paraoxon methyl. The results were compared with that achieved by using the mother Fe_3O_4 nanoparticles. More quantitative results on the signal amplification effect endowed by the controlled aggregation of Fe_3O_4 nanoparticles were extracted by relative optical density analysis. Under optimized conditions, a detection limit of 1.7 ng/mL for paraoxon methyl was achieved by using the particle aggregates, which is almost 40-fold lower than that based on the mother Fe_3O_4 nanoparticles.

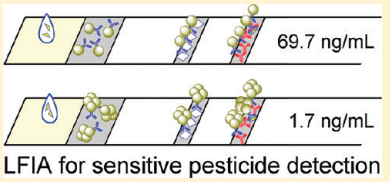

The lateral flow immunochromatographic assay (LFIA), also known as lateral flow tests, is a solid-phase immunoassay combining the principles of thin layer chromatography and immune recognition reaction. Colored particles such as colloidal gold,[1,2] colloidal selenium,[3,4] colloidal carbon,[5] latex,[6] liposome,[7] quantum dot,[8,9] etc. are used as labels of antibody to detect the presence of target analyte. In comparison with the laboratory-oriented instrumental analysis, LFIA is a simple, fast-response, and inexpensive technique useful for medical diagnosis,[10,11] home testing,[12] point of care testing,[13] and detection of various environmental and agricultural contaminations[14−17] as well. Among the aforementioned colored particles, colloidal gold is widely adopted due to its vivid color, caused by localized surface plasmon resonance, and excellent chemical stability.[18] Upon competitive or sandwich type assays, the Au particles labeled by antibody flow along a thin solid matrix together with the analytes driven by capillary force and eventually accumulate upon immune recognition at a defined area pretreated by antibody or antigen. Thus qualitative or semiquantitative detection of various analytes is thus realized by colorimetry read either by naked eyes or with the aid of optical density analysis.[19,20] So far, LFIA based on gold colloidal particles has been demonstrated to be potentially useful for detecting viruses,[21] bacteria,[22] drugs,[1] hormones,[23] environmental pollutants,[24] and etc. The detection limit and sensitivity of the colloidal gold immunochromatography are intrinsically determined by the molar absorption coefficient of Au nanoparticle and its accumulating ability caused by unit analyte. Though colloidal gold particle has relatively high absorption coefficient, the detection limit of Au-based LFIA remains to be improved for detecting trace analytes of being highly hazardous.

An effective way for improving the detection limit of the colloidal gold immunochromatography is to amplify the Au signal by the following immunogold silver staining (IGSS). Because silver is prone to grow on the surface of Au particles, the color of the detection lines caused by Au particles primarily accumulated upon immune recognition is greatly enhanced due to the silver deposition. Cho et al. reported an IGSS-based cross-flow chromatographic assay for detecting cardiac troponin I and the detection sensitivity was demonstrated to be increased by 51-fold in comparison with the conventional LFIA.[25] An alternative approach for enhancing the detection limit is to introduce secondary Au particles to bind with the primarily accumulated Au particles on detection lines. For example, with dependence on the recognition between the bovine serum albumin (BSA)-capped Au particles precaptured in detection zones and anti-BSA antibody-labeled Au particles, the accumulation of Au particles was greatly enhanced and consequently the sensitivity of detecting troponin I was increased by about 100-fold.[26] Although the above-mentioned techniques are effective for signal amplification, they both are characterized by two-step processes and therefore are more complicated than the conventional LFIA.

An interesting attempt was carried out recently by Knopp and co-workers upon the use of composite particles, formed by immobilizing gold particles on magnetic particles, instead of the conventional Au colloids.[27] Although the detection limit achieved for aflatoxin B_2 was only improved by a factor of 3, this study suggests that using the collective effect of colored particles occurring in the form of aggregates may become an effective measure for increasing the sensitivity of the conventional single-step LFIA.

Received: June 9, 2011
Accepted: July 27, 2011
Published: July 27, 2011

Scheme 1. Schematic Drawings for the Preparation of Fe_3O_4 Agregates (Upper Panel), LFIA Principle Based on Fe_3O_4 Particles and Their Aggregates (Middle Panel), and the Structure of a LFIA Strip Together with the Illustrations for Detecting Results (Lower Panel)

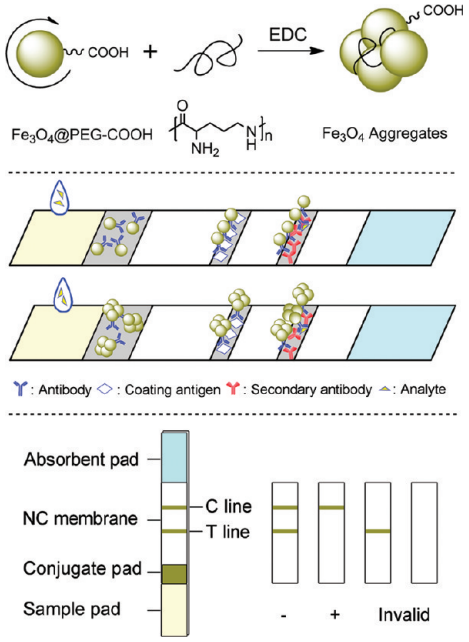

Inspired by these previous investigations, herein we report a sensitive magnetic lateral flow immunochromatographic assay based on magnetic Fe_3O_4 nanoparticles. The general strategy is to use aggregates of Fe_3O_4 nanoparticles as colored reagents instead of individual particles as shown in Scheme 1. In fact, magnetic iron oxide particles have already been reported as colored particles for LFIA in a number of publications.[28−32] The disadvantage of iron oxide particles in comparison with Au particles is that the absorption spectrum of magnetic iron oxide particles is featureless covering almost the whole visible range due to the intraband transition. Therefore, nanometer-sized magnetic iron oxide particles such as Fe_3O_4 nanoparticles present a dark brown color which is apparently not as vivid as that of the colloidal Au. Nevertheless, the integral molar absorption coefficient of Fe_3O_4 nanocrystals within the visible light range is rather comparable to that of the Au nanoparticles. Moreover, the aggregation hardly changes the absorption properties of iron oxide nanoparticles as it does for colloidal Au particles due to the electronic coupling between Au particles in the aggregation state.[18] The other advantage of magnetic iron oxide nanoparticles is that they offer the possibility for trace analyte detection via magnetic signal measurements in addition to optical density analysis.

Following on from our previous investigations on the preparation and bioapplication of Fe_3O_4 nanoparticles,[33−36] poly(ethylene glycol) (PEG)-modified Fe_3O_4 nanoparticles were prepared. Fe_3O_4 nanoparticle aggregates with different hydrodynamic sizes were prepared by cross-linking the Fe_3O_4 nanoparticles bearing carboxyl groups with poly-L-lysine (PLL). The resultant particle aggregates, after being covalently coupled with antiparaoxon methyl polyclonal antibody, were employed as color reagents for LFIA of paraoxon methyl which was chosen as a model compound for pesticide residue. The detection limit achieved was compared with that obtained by either the mother particles or colloidal Au particles.

EXPERIMENTAL SECTION

Reagents and Materials. 1-Ethyl-3-(3-dimethylaminopropyl) carbodiimide hydrochloride (EDC, Pierce, 22980), *N*-hydroxysulfosuccinimide sodium salt (sulfo-NHS, Fluka, 56485), and poly-L-lysine (PLL, M_w 30−70 kDa, Sigma, 25988-63-0) were used as received. Bovine serum albumin (BSA, M_w 67 kDa, purity ≥98%, biotechnology grade) and polyoxyethylene lauryl ether (Brij35) were purchased from Biodee Biotechnology Beijing, Co., Ltd. Ovalbumin (OVA, M_w 45 kDa) was purchased from Boao Biotechnology Shanghai, Co., Ltd. Polyoxyethylene sorbitan monolaurate (Tween-20) and sucrose were obtained from Sinopharm Chemical Reagent Beijing, Co., Ltd. Parathion, methamidophos, chlorpyrifos, carbofuran, and carbaryl were purchased from National Research Center for Certified Reference Materials. Paraoxon methyl was purchased from Dr. Ehrenstorfer (Augsburg, Germany). Goat antirabbit IgG was purchased from Solarbio Science & Technology Co., Ltd. The nitrocellulose membrane (Sartorius CN 140), glass fiber (Ahlstrom 8964 and GF-06) and absorbent paper were purchased from Jiening Biotech Shanghai, Co., Ltd.

Preparation of Magnetic Fe_3O_4 Particle Aggregates. PEG-coated Fe_3O_4 nanoparticles with surface reactive carbonyl moieties were prepared according to a previous publication.[35] The average diameter of the as-prepared particles was of 10.1 ± 1.5 nm determined by transmission electron microscopy (TEM). The synthesis of the Fe_3O_4 aggregates was performed as follows: different amounts of PLL were first mixed with 1 mg of Fe_3O_4 in 1.5 mL of 1× PBS solution containing 10 mM sodium phosphate and 137 mM NaCl and then 0.5 mg of EDC was introduced. After being incubated at 37 °C for 4 h, the resultant particle aggregates were obtained after removing the unreacted PLL, EDC, and its hydrolyzed products by ultrafiltration using a 100 kDa filter (Millipore) at 8000*g*. Then particle aggregates obtained were subsequently redispersed in 0.5 mL of water and stored at 4 °C before use.

Preparation of Antiparaoxon Methyl Polyclonal Antibody. The paraoxon methyl hapten, immunogen, coating antigen and antiparaoxon methyl polyclonal antibody were prepared according to the previous literature.[37] In brief, a paraoxon methyl hapten was designed by replacing the nitryl group with a propionic acid group. It was synthesized and then used to conjugate to BSA and OVA for preparing immunogen and coating antigen, respectively. The polyclonal antibody was obtained by immunizing rabbits with the paraoxon methyl hapten-BSA.

Preparation of Fe_3O_4 Particle Aggregate-Antibody Conjugates. The conjugates of Fe_3O_4 nanoparticle aggregates and antiparaoxon methyl polyclonal antibody were prepared by (EDC/sulfo-NHS)-mediated amidation reaction. Typically, 0.83 μmol of EDC and 2.25 μmol of sulfo-NHS were dissolved in 160 μL of 1× PBS buffer solution containing 0.32 mg of Fe_3O_4 nanoparticles. After approximately 15 min, 25.4 μL of 1× PBS buffer solution containing 0.084 mg of paraoxon methyl polyclonal antibody was introduced. The reaction lasted for 4 h at 37 °C under gentle mixing. Then the resultant mixture was stored at 4 °C overnight. No further purification was carried out before use. The conjugation reactions between differently sized

dx.doi.org/10.1021/ac201462d |*Anal. Chem.* 2011, 83, 6778–6784

particle aggregates and antibody were carried out in quite a similar way.

Magnetic Lateral Flow Immunochromatographic Assay. The 3 mm-wide LFIA strip consists of five components including a sample pad for applying sample solution, a conjugate pad for loading the particle-labeled antibody, a 25 mm long nitrocellulose (NC) membrane acting as the chromatography matrix, an absorbent pad serving as the liquid sink, and a backing card for supporting all the components. Typically, at 5 mm from the absorbent pad, a band of goat antirabbit IgG (1 mg/mL) was manually drawn on the NC membrane as a control line (C-line), while a band of coating antigen (paraoxon methyl hapten-OVA) (0.4 mg/mL) was drawn as the test line (T-line) 10 mm from the conjugate pad. Typically, the sample pad of 3 mm × 20 mm was pretreated by 1× PBS buffer containing 0.4% (w/v) Brij-35, and the conjugate pad of 3 mm × 5 mm was pretreated by PBS buffer containing 0.1% (w/v) BSA, 0.05% (w/v) Tween 20, and 10% (w/v) sucrose, respectively. Then, 2 μL solution of the as-prepared particle-antibody conjugate was spotted on the conjugate pad. After the aforementioned LIFA components were dried properly, they were assembled with the overlaps between the sample pad and conjugate pad and that between the conjugate pad and the NC membrane being 2 mm to ensure the solution is migrating properly through the strip during the detection.

The following LFIA experiments upon competitive assay were run as follows. In brief, 100 μL solution of paraoxon methyl with a series of concentrations in 1× PBS buffer was applied to the sample pad in a controlled environment with the relative humidity of 40−50%. Then, the relative optical density of both test line and control line was acquired 15 min later.

To evaluate the specificity of the current detection method for paraoxon methyl, five commonly used pesticides, such as parathion, methamidophos, chlorpyrifos, carbofuran, and carbaryl, were chosen as controls. The standard solutions of these pesticides with concentrations of 100, 500, and 1000 ng/mL were prepared by diluting the corresponding stock solutions (100 μg/mL, in acetone) with 1× PBS. The following LFIA experiments were carried out in the same way as mentioned above for paraoxon methyl.

Characterizations. Dynamic light scattering was carried out at 298.0 K with a Zetasizer Nano ZS (Malvern) equipped with a solid-state He−Ne laser (λ = 633 nm) for monitoring the variation of the hydrodynamic size of the magnetic nanoparticles before and after being cross-linked by PLL. TEM measurements were carried out with a JEM-100CXII microscope operating at an accelerating voltage of 100 kV for characterizing the magnetic nanoparticles and their aggregates. The optical image of the test strips was acquired by using a Canon IXUS80IS camera and then processed by using ImageJ 1.42q software for analyzing the optical density of the test and control lines.

RESULTS AND DISCUSSION

The general strategy reported herein for sensitive detection of pesticide residues is to use particle aggregates as the color reagents of LFIA instead of individual particles. To prove this concept, the PEG-coated Fe_3O_4 nanoparticles with surface reactive carbonyl moieties were adopted due to the fact that they have received intensive investigations and been demonstrated to be able to form Fe_3O_4-antibody probes via amidation reaction.[34,35] Following similar approach, via the surface reactive

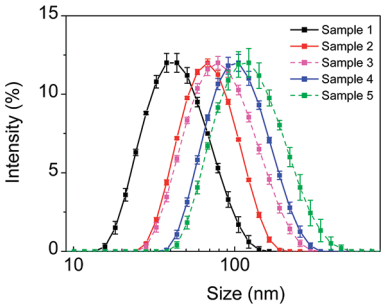

Figure 1. The hydrodynamic size distribution profiles of Fe_3O_4 particle aggregate samples (samples 1−5) with more detailed DLS results being provided in Table 1.

carbonyl moieties, the aggregates of Fe_3O_4 nanoparticles were prepared by cross-linking the individual nanoparticles with PLL that possesses an amine group in each repeat unit. Dynamic light scattering technique was adopted to reveal the variations in size and size distributions of the particle aggregates obtained upon different Fe_3O_4/PLL ratios by plotting the hydrodynamic size vs relative light scattering intensity as shown Figure 1. The detailed results are provided in Table 1. In comparison with the mother Fe_3O_4 nanoparticles, the particle aggregates present similar size distribution profiles with the central peak position moving toward large size against the amount of PLL. Most importantly, the appearance of single light scattering peak in each aggregate sample implies that neither unwanted coagulation nor huge agglomeration appeared during the preparation of the particle aggregates. All these results suggest that the aggregates of Fe_3O_4 nanoparticles can be produced in a controllable way within the Fe_3O_4/PLL ratio range given in Table 1. Further increasing the amount of PLL led to polydispered particle aggregates with poor colloidal stability under ambient conditions, as shown in Figure S1 in the Supporting Information. Therefore, three aggregate samples with a hydrodynamic size of 47.3 nm (sample 1), 77.9 nm (sample 2), and 113.6 nm (sample 4), respectively, were chosen as labels in the following LFIAs. Ethylene diamine was also used to cross-link the Fe_3O_4 nanoparticles, but it is difficult to achieve particle aggregates larger than 70 nm (Figure S2 in the Supporting Information) due to the short chain length between two amine groups.

TEM investigations were carried out to further characterize the particle aggregates. As shown in Figure 2a, the mother Fe_3O_4 nanoparticles occur in a rather dispersed state when the solution of particles used for TEM sample preparation is dilute enough, although they tend to form a close-packed structure when the concentration of the mother particles is increased, as shown in the inset of Figure 2a. In contrast, even by dilution, samples 2 and 4 remain appearing as isolated aggregates of particles as shown in parts b and c of Figure 2, respectively. In comparison with sample 2, the aggregates in sample 4 are comprised of more Fe_3O_4 nanoparticles, which is consistent with the DLS results shown in Figure 1, although the particle aggregates tend to form catenulate rather than spherical structures.

The conjugation between antiparaoxon methyl polyclonal antibody and the Fe_3O_4 particle aggregates was realized by amidation reaction mediated by EDC and sulfo-NHS, assuming that there are still carbonyl groups on the magnetic nanoparticles being available though part of them will be used for forming the particle aggregates by reacting with PLL. It is difficult to detect the availability of the surface carbonyl groups on the resultant

dx.doi.org/10.1021/ac201462d |*Anal. Chem.* 2011, 83, 6778–6784

Table 1. Feeding Amounts of Fe_3O_4 and PLL for Preparing Particle Aggregates (Samples 2−5) Together with the Detailed DLS Results for Both Aggregate Samples and the Mother Fe_3O_4 Particles (Sample 1)

	sample 1	sample 2	sample 3	sample 4	sample 5
Fe_3O_4 (mg)	0.978	0.978	0.978	0.978	0.978
PLL (mg)	0	7.80×10^{-4}	4.78×10^{-3}	7.80×10^{-3}	1.56×10^{-2}
Z avg (nm)	42.8	66.0	77.5	101.0	115.0
size by intensity (nm)	47.3	77.9	90.8	113.6	137.1
size by number (nm)	22.9	36.5	41.1	56.1	64.3
ζ potential (mV)	−5.3	−6.12	−6.48	−6.75	−6.78

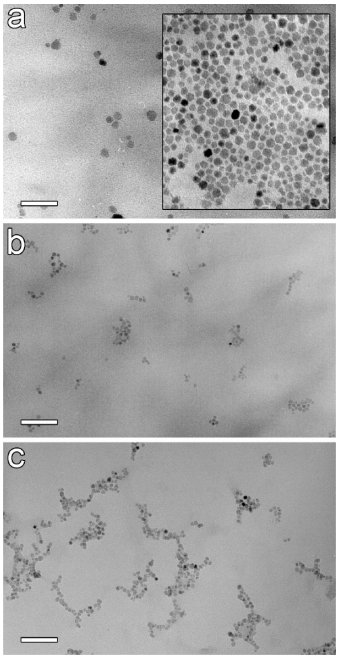

Figure 2. TEM images of sample 1 (a), sample 2 (b), and sample 4 (c). The inset shows the mother Fe_3O_4 nanoparticles in a closely packed stage. The scale bars correspond to 50 (a) and 100 nm (b and c), respectively.

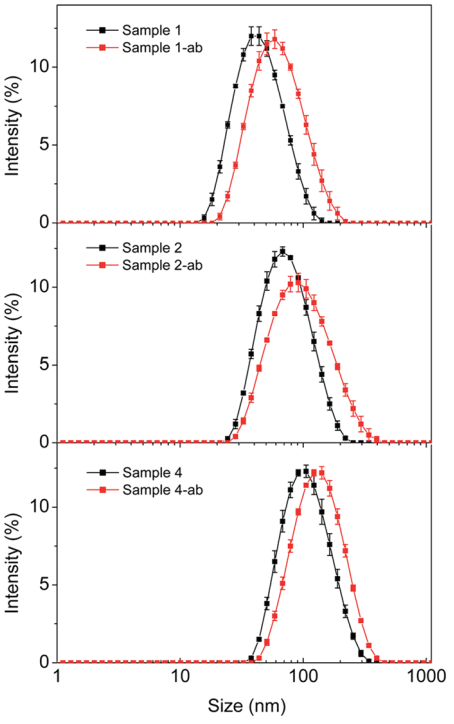

Figure 3. The hydrodynamic size distribution profiles of different particle samples recorded before (denoted as samples 1, 2, 4) and after the conjugation reaction with antibody (denoted as samples 1-ab, 2-ab, and 4-ab, respectively).

aggregate by conventional spectroscopy. Therefore DLS investigations were adopted to confirm the conjugation reaction between the Fe_3O_4 particles (samples 1, 2, and 4) and antibody by determining the size variation of the particles after the conjugation reaction. The results in Figure 3 show that the intensity-weighted mean hydrodynamic sizes of the conjugates, denoted as sample 1-ab, sample 2-ab, and sample 4-ab, are 67.3, 107.7, and 143.0 nm, respectively. In comparison with the corresponding mother particle aggregates, the hydrodynamic size of the resultant conjugates is increased by 20−30 nm. Taking 10 nm for the average hydrodynamic size of IgG (150 kDa),[38] the reasonable increment in the hydrodynamic size after the coupling reaction supports that the antibody molecules are effectively coupled to all three particle samples via the amidation reaction. In addition, the coupling reactions took place in a controllable way as no additional light scattering peaks appears.

In the following LFIA experiments, the paraoxon methyl (M_w = 247.14) detection was performed by using the bioconjugates mentioned above, i.e., sample 1-ab, sample 2-ab, and sample 4-ab via competitive assay. The detection principle is given below. When an aqueous solution of target analyte is applied onto the sample pad, the particle-antibody conjugates are rehydrated, consequently released into the migrating liquid and then migrate across both the T-line and C-line driven by capillary force. As both paraoxon methyl in solution and the paraoxon methyl residue immobilized via OVA on the T-line can specifically bind with the particle-antibody conjugates, as shown in Scheme 1, they will be in competition to bind to the limited binding sites on the particle-antibody conjugates. Consequently, the color of the T-line, determined by the amount of the colored particles, inversely reflects the amount of target analyte. In contrast, all particles that migrate across the C-line will be captured by the secondary antibody immobilized on the C-line, independent of the combination between the analyte and the colored particles. Therefore, the color of the C-line reflects the effective release of the particle-antibody conjugates from the conjugate pad and is used for testing the validity of the run.

Figure 4 shows the typical responses of the magnetic LFIA to paraoxon methyl with increasing concentrations from 0 to 5000 ng/mL under optimal conditions based on sample 1-ab (panel a),

dx.doi.org/10.1021/ac201462d |*Anal. Chem.* 2011, 83, 6778–6784

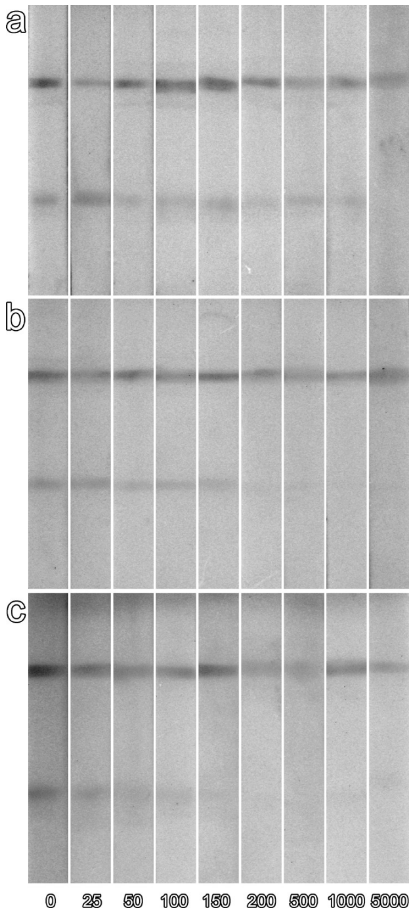

Figure 4. The photographs of test strips of LFIA based on different particles, i.e., sample 1 (a), sample 2 (b), and sample 4 (c). The concentration unit for those shown on the bottom is nanogram/milliliter.

sample 2-ab (panel b), and sample 4-ab (panel c), respectively. The visual detection limit is defined herein as the minimum target analyte concentration required by the T-line for showing no obvious staining effect. Following this definition, the visual detection limit achieved by sample 1-ab is above 1000 ng/mL, quite comparable with colloidal Au LFIA achieved under optimal conditions as shown in Figure S3 in the Supporting Information. In contrast, the detection limit achieved by samples 2-ab and 4-ab is around 200 and 150 ng/mL, respectively, greatly decreased in comparison with that achieved by the mother Fe_3O_4 nanoparticles, strongly supporting that using the particle aggregates is an effective way to achieve highly sensitive LFIA. Although a lower detection limit of 100 ng/mL was also achieved as shown in Figure S4 in the Supporting Information by using particle aggregates with a larger size, e.g., sample 5, the release and migration of the resultant probe were less effective in comparison with those shown in Figure 4 due to the reduced colloidal stability of sample 5.

In order to quantitatively extract the detection limit of the current LFIA method, the test strips were further subjected to optical density analysis. A series of paraoxon methyl solutions with concentrations of 0, 1, 10, 25, 50, 100, 150, 200, 500, 1000, and 5000 ng/mL in 1× PBS buffer were prepared and used in the following experiments based on the particle-antibody conjugate of sample 4. The signals on both the T-line and C-line averaged from

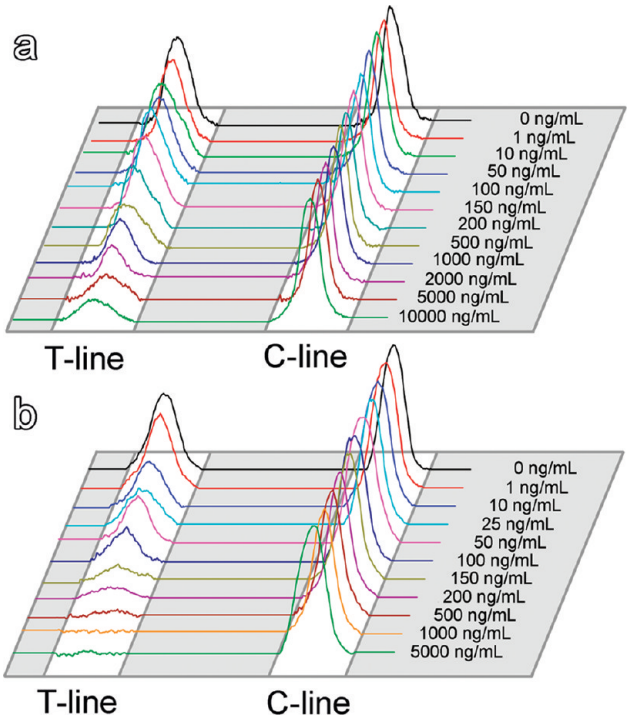

Figure 5. Optical density profiles of the T-line and C-line recorded by using sample 1-ab (a) and sample 4-ab (b) after running a series of standard solutions with different paraoxon methyl concentrations.

five parallel runs were digitized to optical density using software of ImageJ and expressed by integral area of the cross-section of the T-line ($area_T$) and C-line ($area_C$) within a fixed peak width. In order to eliminate the influence of artificial effects, a relative optical density (ROD) defined as $area_T/area_C$ was used in the signal analysis. For comparison, the same analysis was also applied to quantify the results obtained upon the use of the mother particles (sample 1) for showing the contribution of the aggregation of the particles to the sensitivity of LFIA. The optical density profiles of both the T-line and C-line recorded under different analyte concentrations are shown in Figure 5 with the optical density of the T-line being normalized with respect to that of the C-line. The optical intensity of the T-line is quite obviously increased with the decrease of the analyte concentration, and this tendency is clearly enhanced by using the particle aggregates (panel b, sample 4) instead of individual particles (panel a, sample 1).

To extract the detection limit of the current LFIAs, the ROD of the T-line is plotted against the concentration of paraoxon methyl in the logarithm scale as shown in Figure 6. Linear fitting of the dose−response curves suggests that the linear response range of sample 1-ab is over 3 orders of magnitude from 50 to 5000 ng/mL with a correlation coefficient of 0.9909, while the linear response range of sample 4-ab is also over 3 orders of magnitude but ranging from 1 to 1000 ng/mL with a correlation coefficient of 0.9894. With the definition of the detection limit as the minimum concentration of analyte required for inducing a 10% ROD decrease,[17] as guided by the dashed line, it was determined as 69.7 ng/mL for sample 1-ab and 1.7 ng/mL for sample 4-ab, respectively, suggesting that the detection limit is decreased by more than 40-fold upon the use of particle aggregates instead of individual particles. The decreased detection limit achieved by using particle aggregates can be understood as follows. On the one hand, the immobilization of the

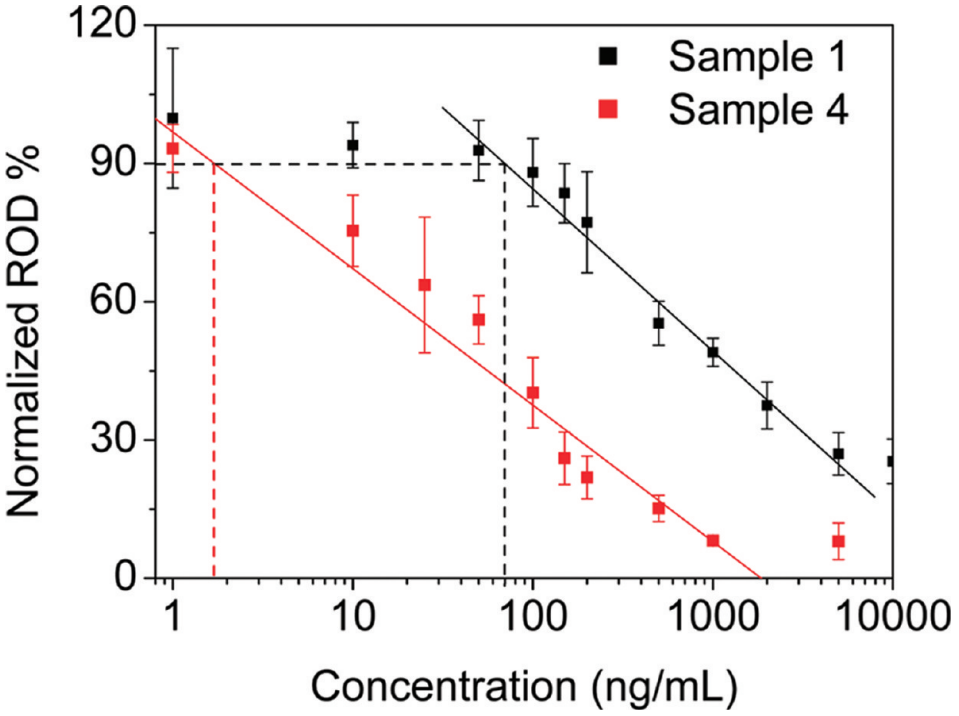

Figure 6. Dose−response curves for paraoxon methyl based on optical density analysis using samples 1 and 4 as labels of the antibody.

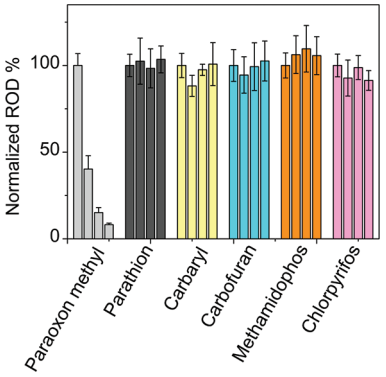

Figure 7. The ROD of different tests based on sample 4-ab for detecting six different types of pesticides with concentrations of 0, 100, 500, and 1000 ng/mL (from left to right).

particle-antibody probe upon the immune recognition is apparently more pronounced with respect to the particle aggregates since one effective binding site will help to hold a large number of individual particles, as shown in Figure S5 in the Supporting Information. On the other hand, the migration velocity of particle aggregates is smaller than individual particles, which is in favor of effective immobilization of iron oxide particles due to the prolonged recognition time and consequently also contributes to the decreased detection limit.

The specificity of the immunoassay is normally associated with the antibody−antigen binding specificity. Apart from that, the impact of particle aggregation on the binding specificity is less known yet. Therefore, the particle probe constructed by sample 4 and the antiparaoxon methyl polyclonal antibody was used in detecting paraoxon methyl with five commonly used pesticides such as parathion, carbaryl, carbofuran, methamidophos, and chlorpyrifos as controls. Four parallel testing runs were carried out in detecting the above pesticides with concentrations of 0, 100, 500, and 1000 ng/mL, respectively. The quantitative results obtained upon optical density analysis are provided in Figure 7. It is quite obvious that none of the control pesticides presents a dose−response relationship even though some of them are structurally similar to paraoxon methyl, which suggests that the controlled aggregation of iron oxide particles does not decrease the detection specificity while improving the detection limit.

CONCLUSIONS

In summary, a highly sensitive and specific magnetic LFIA method is established via the use of Fe_3O_4 particle aggregates instead of individual nanoparticles commonly adopted in conventional LFIA. The key procedure is to achieve controllable Fe_3O_4 particle aggregates that are obtained by cross-linking the PEG-coated Fe_3O_4 nanoparticles bearing surface reactive carbonyl moieties with PLL upon a suitable Fe_3O_4 to PLL ratio. Because of the significant amplification effect, the Fe_3O_4 particle aggregates offer a greatly improved visual detection limit in detecting the paraoxon methyl, in addition to excellent detection specificity. More quantitative analysis through relative optical density demonstrates that the detection limit is decreased by more than 40-fold, reaching 1.7 ng/mL. The current investigations thereby pave a novel strategy for developing ultrasensitive LFIA through the amplification effect endowed by the controlled particle aggregation. Moreover, the current method may provide a highly sensitive detection method for hazardous substances through magnetic signal detection on Fe_3O_4 particle aggregates.

ASSOCIATED CONTENT

Supporting Information. Additional information as noted in text. This material is available free of charge via the Internet at http://pubs.acs.org.

AUTHOR INFORMATION

Corresponding Author

*E-mail: gaomy@iccas.ac.cn (M.G.); wanglb1@163.com (L.W.). Fax: +86 10 8261 3214 (M.G.).

ACKNOWLEDGMENT

The current investigations are jointly supported by 863 Project (Grant 2010AA06Z302), NSFC Projects (Grant 20903 100), and the National Basic Research Program of China (Grant 2011CB935800).

REFERENCES

(1) Verheijen, R.; Stouten, P.; Cazemier, G.; Haasnoot, W. *Analyst* **1998**, *123*, 2437–2441.
(2) Shyu, R. H.; Shyu, H. F.; Liu, H. W.; Tang, S. S. *Toxicon* **2002**, *40*, 255–258.
(3) Osikowicz, G.; Beggs, M.; Brookhart, P.; Caplan, D.; Ching, S. F.; Eck, P.; Gordon, J.; Richerson, R.; Sampedro, S.; Stimpson, D.; Walsworth, F. *Clin. Chem.* **1990**, *36*, 1586–1586.
(4) Lou, S. C.; Patel, C.; Ching, S. F.; Gordon, J. *Clin. Chem.* **1993**, *39*, 619–624.
(5) Lönnberg; Carlsson, J. *Anal. Biochem.* **2001**, *293*, 224–231.
(6) Birnbaum, S.; Udén, C.; Magnusson, C. G. M.; Nilsson, S. *Anal. Biochem.* **1992**, *206*, 168–171.
(7) Gussenhoven, G. C.; van der Hoorn, M. A. W. G.; Goris, M. G. A.; Terpstra, W. J.; Hartskeerl, R. A.; Mol, B. W.; van Ingen, C. W.; Smits, H. L. *J. Clin. Microbiol.* **1997**, *35*, 92–97.
(8) Liu, G. D.; Lin, Y. Y.; Wang, J.; Wu, H.; Wai, C. M.; Lin, Y. H. *Anal. Chem.* **2007**, *79*, 7644–7653.
(9) Zou, Z. X.; Du, D.; Wang, J.; Smith, J. N.; Timchalk, C.; Li, Y. Q.; Lin, Y. H. *Anal. Chem.* **2010**, *82*, 5125–5133.
(10) Schramm, W.; Angulo, G. B.; Torres, P. C.; Burgess-Cassler, A. *Clin. Diagn. Lab. Immunol.* **1999**, *6*, 577–580.
(11) Fernández-Sánchez, C.; McNeil, C. J.; Rawson, K.; Nilsson, O. *Anal. Chem.* **2004**, *76*, 5649–5656.
(12) Elkjaer, M.; Burisch, J.; Hansen, V. V.; Kristensen, B. D.; Jensen, J. K. S.; Munkholm, P. *Aliment. Pharm. Therap.* **2010**, *31*, 323–330.
(13) Laderman, E. I.; Whitworth, E.; Dumaual, E.; Jones, M.; Hudak, A.; Hogrefe, W.; Carney, J.; Groen, J. *Clin. Vaccine Immunol.* **2008**, *15*, 159–163.
(14) Zhou, P.; Lu, Y. T.; Zhu, J.; Hong, J. B.; Li, B.; Zhou, J.; Gong, D.; Montoya, A. *J. Agric. Food Chem.* **2004**, *52*, 4355–4359.
(15) Delmulle, B. S.; De Saeger, S.; Sibanda, L.; Barna-Vetro, I.; Van Peteghem, C. H. *J. Agric. Food Chem.* **2005**, *53*, 3364–3368.
(16) Molinelli, A.; Grossalber, K.; Füehrer, M.; Baumgartner, S.; Sulyok, M.; Krska, R. *J. Agric. Food Chem.* **2008**, *56*, 2589–2594.
(17) Blažková, M.; Mičová-Holubová, B.; Rauch, P.; Fukal, L. *Biosens. Bioelectron.* **2009**, *25*, 753–758.
(18) Li, C. M.; Li, Y. F.; Wang, J.; Huang, C. Z. *Talanta* **2010**, *81*, 1339–1345.
(19) Zhang, G. P.; Wang, X. N.; Yang, J. F.; Yang, Y. Y.; Xing, G. X.; Li, Q. M.; Zhao, D.; Chai, S. J.; Guo, J. Q. *J. Immunol. Methods* **2006**, *312*, 27–33.
(20) Cho, I. H.; Paek, E. H.; Kim, Y. K.; Kim, J. H.; Paek, S. H. *Anal. Chim. Acta* **2009**, *632*, 247–255.
(21) Vaughn, D. W.; Nisalak, A.; Kalayanarooj, S.; Solomon, T.; Dung, N. M.; Cuzzubbo, A.; Devine, P. L. *J. Clin. Microbiol.* **1998**, *36*, 234–238.
(22) Grunow, R.; Splettstoesser, W.; McDonald, S.; Otterbein, C.; O'Brien, T.; Morgan, C.; Aldrich, J.; Hofer, E.; Finke, E. J.; Meyer, H. *Clin. Vaccine Immunol.* **2000**, *7*, 86–90.
(23) Leung, W. M.; Chan, P. Y.; Bosgoed, F.; Lehmann, K.; Renneberg, K.; Lehmann, M.; Renneberg, R. *J. Immunol. Methods* **2003**, *281*, 109–118.
(24) Zhu, J.; Chen, W. C.; Lu, Y. T.; Cheng, G. H. *Environ. Pollut.* **2008**, *156*, 136–142.
(25) Cho, I. H.; Seo, S. M.; Paek, E. H.; Paek, S. H. *J. Chromatogr., B* **2010**, *878*, 271–277.
(26) Choi, D. H.; Lee, S. K.; Oh, Y. K.; Bae, B. W.; Lee, S. D.; Kim, S.; Shin, Y. B.; Kim, M. G. *Biosens. Bioelectron.* **2010**, *25*, 1999–2002.
(27) Tang, D.; Sauceda, J. C.; Lin, Z.; Ott, S.; Basova, E.; Goryacheva, I.; Biselli, S.; Lin, J.; Niessner, R.; Knopp, D. *Biosens. Bioelectron.* **2009**, *25*, 514–518.
(28) Wang, Y. Y.; Xu, H.; Wei, M.; Gu, H. C.; Xu, Q. F.; Zhu, W. *Mater. Sci. Eng., C* **2009**, *29*, 714–718.
(29) Workman, S.; Wells, S. K.; Pau, C. P.; Owen, S. M.; Dong, X. F.; LaBorde, R.; Granade, T. C. *J. Virol. Methods* **2009**, *160*, 14–21.
(30) Taton, K.; Johnson, D.; Guire, P.; Lange, E.; Tondra, M. *J. Magn. Magn. Mater.* **2009**, *321*, 1679–1682.
(31) Handali, S.; Klarman, M.; Gaspard, A. N.; Dong, X. F.; LaBorde, R.; Noh, J.; Lee, Y. M.; Rodriguez, S.; Gonzalez, A. E.; Garcia, H. H.; Gilman, R. H.; Tsang, V. C. W.; Wilkins, P. P. *Clin. Vaccine Immunol.* **2010**, *17*, 631–637.
(32) Peck, R. B.; Schweizer, J.; Weigl, B. H.; Somoza, C.; Silver, J.; Sellors, J. W. *Clin. Chem.* **2006**, *52*, 2170–2172.
(33) Li, Z.; Wei, L.; Gao, M. Y.; Lei, H. *Adv. Mater.* **2005**, *17* 1001–1005.
(34) Hu, F. Q.; Wei, L.; Zhou, Z.; Ran, Y. L.; Li, Z.; Gao, M. Y. *Adv. Mater.* **2006**, *18*, 2553–2556.
(35) Liu, S. J.; Jia, B.; Qiao, R. R.; Yang, Z.; Yu, Z. L.; Liu, Z. F.; Liu, K.; Shi, J. Y.; Han, O. Y.; Wang, F.; Gao, M. Y. *Mol. Pharmaceutics* **2009**, *6*, 1074–1082.
(36) Liu, S. J.; Han, Y. C.; Qiao, R. R.; Zeng, J. F.; Jia, Q. J.; Wang, Y. L.; Gao, M. Y. *J. Phys. Chem. C* **2010**, *114*, 21270–21276.
(37) Li, Z. K.; Zhu, Y. Y.; Yin, X. G.; Peng, C. F.; Chen, W.; Liu, L. Q.; Yin, L. M.; Xu, C. L. *Immunol. Invest.* **2009**, *38*, 510–525.
(38) Jans, H.; Liu, X.; Austin, L.; Maes, G.; Huo, Q. *Anal. Chem.* **2009**, *81*, 9425–9432.